Solvent effects on the ultrafast nonradiative deactivation mechanisms of thymine in aqueous solution: Excited-state QM/MM molecular dynamics simulations

Akira Nakayama, Gaku Arai, Shohei Yamazaki, and Tetsuya Taketsugu

Citation: The Journal of Chemical Physics **139**, 214304 (2013); doi: 10.1063/1.4833563
View online: http://dx.doi.org/10.1063/1.4833563
View Table of Contents: http://scitation.aip.org/content/aip/journal/jcp/139/21?ver=pdfcov
Published by the AIP Publishing

Solvent effects on the ultrafast nonradiative deactivation mechanisms of thymine in aqueous solution: Excited-state QM/MM molecular dynamics simulations

Akira Nakayama,[a] Gaku Arai, Shohei Yamazaki,[b] and Tetsuya Taketsugu
Department of Chemistry, Faculty of Science, Hokkaido University, Sapporo 060-0810, Japan

(Received 7 May 2013; accepted 12 November 2013; published online 3 December 2013)

On-the-fly excited-state quantum mechanics/molecular mechanics molecular dynamics (QM/MM-MD) simulations of thymine in aqueous solution are performed to investigate the role of solvent water molecules on the nonradiative deactivation process. The complete active space second-order perturbation theory (CASPT2) method is employed for a thymine molecule as the QM part in order to provide a reliable description of the excited-state potential energies. It is found that, in addition to the previously reported deactivation pathway involving the twisting of the C-C double bond in the pyrimidine ring, another efficient deactivation pathway leading to conical intersections that accompanies the out-of-plane displacement of the carbonyl group is observed in aqueous solution. Decay through this pathway is not observed in the gas phase simulations, and our analysis indicates that the hydrogen bonds with solvent water molecules play a key role in stabilizing the potential energies of thymine in this additional decay pathway. © *2013 AIP Publishing LLC*. [http://dx.doi.org/10.1063/1.4833563]

I. INTRODUCTION

Ultrafast nonradiative decay of DNA bases after UV-irradiation is an essential defense mechanism against photo-damage, and much effort has been devoted to the understanding of the underlying mechanisms at the molecular level.[1–4] It is now well-known that the conical intersection (CI) points between the ground- and excited-state potential energy surfaces play a crucial role in dissipating the energy attained by photo-excitation[5,6] and that this process occurs very fast ranging from the subpicosecond to picosecond timescale. The interplay between experiments and theoretical calculations continues to aid in the elucidation of the decay mechanisms, and the intricate dynamics of DNA bases are being rapidly unraveled.

Current challenges are to understand how the complex environments affect the relaxation dynamics of DNA bases, or in other words, play an active role in altering the relaxation dynamics. Most of theoretical calculations so far have focused on the deactivation process in the gas phase by exploring the excited-state potential energy surfaces. Dynamics simulations in the gas phase employing the on-the-fly evaluation of the potential energy are also performed extensively in order to obtain a time-dependent picture of the relaxation dynamics.[7–11] However, dynamical behaviors of DNA bases in complex environments such as in solution phase or in double-stranded DNA environments are still poorly understood.

Thymine has been under active investigation for a long time both experimentally and theoretically. In the gas phase, basically three transients are observed in time-resolved spectra,[12–19] which represent the decays of the excited-state population, and they are ranging from the femtosecond to nanosecond domain. The assignment of these transients are still disputed even in the gas phase, but at least the involvement of two excited states, the bright $^1\pi\pi^*$ and dark $^1n\pi^*$ states, is almost conclusively accepted.[20] Theoretical calculations suggested that the subpicosecond component corresponds to the direct decay in the bright $^1\pi\pi^*$ state leading to CI involving the twisting of the C5-C6 (for the atomic labeling, see Figure 1) double bond in the pyrimidine ring.[9,21–24] These calculations have also shown that a state switch to the $^1n\pi^*$ state is deemed to be responsible for the long-time components. The intersystem crossing to the triplet manifolds was also proposed by Serrano-Pérez *et al.*,[25] as another origin of the long-time components.

Time-resolved spectroscopic experiments of thymine in solution phase have been also performed extensively.[1,20,26–28] In particular, Gustavsson *et al.* measured the excited-state lifetime of thymine using femtosecond UV fluorescence upconversion in various protic and aprotic polar environments.[26–28] They observed an ultrafast component (<100 fs) and also longer component that exhibited a large solvent dependency. The ultrafast excited-state lifetime constant was also observed in the gas phase, but the lifetime of the longer component (e.g., 0.63 ps in aqueous solution) was found to be shorter in polar environments than in the gas phase (5–9 ps).[12,15–19] Also, it was reported that the relative weights of the two components exhibited no clear correlation to bulk solvent polarity and viscosity.[26] These observations imply that molecular-level interaction with solvent may play a significant role in the nonradiative decay of thymine in solution phase. Despite the enormous efforts, however, the underlying mechanism is far from being fully understood.

[a] Author to whom correspondence should be addressed. Electronic mail: nakayama@cat.hokudai.ac.jp. Present address: Catalysis Research Center, Hokkaido University, Sapporo 001-0021, Japan.
[b] Present address: Department of Frontier Materials Chemistry, Graduate School of Science and Technology, Hirosaki University, Hirosaki 036-8561, Japan.

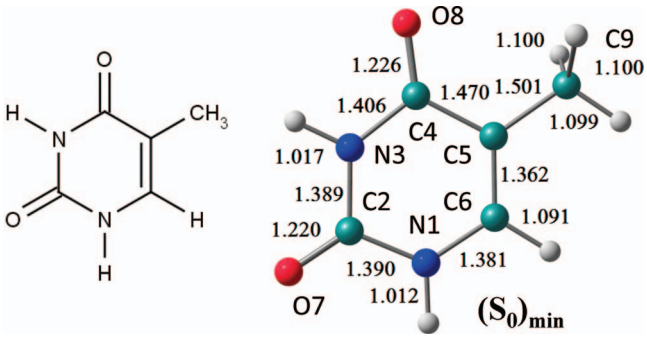

FIG. 1. (Left) Molecular structure of thymine. (Right) Equilibrium structure of thymine in the electronic ground state obtained by the MP2 calculation. Bond lengths are given in units of Å.

In this work we examine the relaxation dynamics of thymine in aqueous solution, highlighting the role of solvent water molecules in the nonradiative deactivation process. We perform the on-the-fly excited-state quantum mechanics/molecular mechanics molecular dynamics (QM/MM-MD) simulations, employing the complete active space second-order perturbation theory (CASPT2) method for a reliable description of the excited-state potential energies of a thymine molecule. The QM-MD simulations corresponding to a situation in the gas phase are also carried out for comparison purposes. As far as we know, it is the first report of the on-the-fly excited-state dynamics simulations of thymine in aqueous solution.

This paper is organized as follows. After presenting the computational details, the deactivation pathways in the $^1\pi\pi^*$ state are examined by exploring the excited-state potential energy surfaces from the Franck-Condon (FC) region to the minimal energy conical intersection (MECI) points. Absorption spectra are calculated in the framework of QM/MM treatment in order to discuss the relative stability of two excited states, the bright $^1\pi\pi^*$ and dark $^1n\pi^*$ states, in aqueous solution. Then, the results of QM-MD and QM/MM-MD simulations are presented and discussed. Finally, some concluding remarks are given.

II. COMPUTATIONAL DETAILS

A. Quantum chemical calculations

We present quantum chemical calculations using the CASPT2 method for the vertical excitation energies at the ground-state equilibrium structure $(S_0)_{min}$ and excited-state potential energy profiles from $(S_0)_{min}$ to the MECI points between the S_0 and $^1\pi\pi^*$ states. The $(S_0)_{min}$ structure is determined by the geometry optimization at the Møller-Plesset second-order perturbation (MP2) level, while the MECI points are located at the CASPT2 level with the penalty function approach.[29] In geometry optimization, no symmetry constraints are imposed. The Sapporo-DZP basis set is used throughout this study.[30] In CASPT2 calculations, the notation of CASPT2(m,n) is used, in which case the active space for a reference state-averaged complete active space self-consistent field (SA-CASSCF) wavefunction is composed of m electrons and n orbitals (SA-CASSCF(m,n)). The vertical excitation energies and potential energy profiles are calculated at the CASPT2(12,9) level, where the active space is comprised of eight π orbitals (five π orbitals are doubly occupied and three are unoccupied in the closed-shell configuration) and one lone-pair orbital that belongs to the O8 atom. A lone-pair orbital on the O7 atom is excluded from the active space, since the $^1n\pi^*$ state involving an excitation from this orbital lies quite high in energy. The S_0, lowest two $^1\pi\pi^*$, and lowest two $^1n\pi^*$ states (a total of five states) are averaged with equal weights in the SA-CASSCF(12,9) calculations. In the MECI geometry optimization, the CASPT2(2,2) or CASPT2(4,4) method is employed for reducing the computational cost, and the details are provided below. We note here that there are two classes of the CASPT2 method: the single-state (SS-) CASPT2[31,32] and multistate (MS-) CASPT2[33] methods. The MS-CASPT2 method is generally recommended for excited-state calculations of DNA bases[24,34] since the SS-CASPT2 method often predicts spurious CIs due to the nonorthogonality of the relevant wavefunctions. The MS-CASPT2 method corrects this artifact by mixing these perturbed states via an effective Hamiltonian approach, although some care is needed when the size of the active space is small for medium-sized systems.[35] In this work, we use the SS-CASPT2 method (referred to as CASPT2) for both the exploration of the excited-state potential energy surfaces and dynamics simulations since an employment of the MS-CASPT2 method is computationally highly demanding, in particular, for dynamics simulations. The validity of the use of the SS-CASPT2 method is examined by comparing with the results of MS-CASPT2 calculations (see below). A level shift with a value of 0.2 is applied for CASPT2 calculations[36] and all quantum chemical calculations are performed by the MOLPRO2008.1 package.[37]

B. Excited-state QM-MD and QM/MM-MD simulations

The excited-state QM-MD and QM/MM-MD simulations are performed to investigate the ultrafast nonradiative deactivation process of thymine in the gas phase and in aqueous solution, respectively. In the QM-MD simulations, a thymine molecule is treated by *ab initio* calculations with the CASPT2 method. In the QM/MM-MD simulations, the QM region is composed of a thymine molecule and treated by *ab initio* calculations also at the CASPT2 level, while the MM region consists of surrounding solvent water molecules that are represented by the SPC/Fw model.[38] The electrostatic interaction of electrons in the QM region with the MM effective point charges is taken into account through one-electron integrals, and the CASPT2 gradients are obtained by the coupled-perturbed equations (CP-CASPT2).[39] The periodic supercell with a length of 16 Å is employed and the thymine molecule is solvated by 122 water molecules. The number of water molecules is determined to reproduce the density of water at ambient conditions. The long-range electrostatic interactions between the MM molecules are treated by the Ewald sum and the cutoff distance of 8 Å (half the length of the supercell) is employed for electrostatic interactions between the QM

(thymine) and MM molecules. Even with this cutoff for electrostatic interactions between the QM and MM molecules, the total energy of the system was well conserved and its standard deviation was ~1.0 kcal/mol for all excited-state MD trajectories. The quantum chemistry package MOLPRO2008.1 is used for *ab initio* calculations and it is interfaced with the in-house MD program to perform QM/MM-MD simulations.

As a computational level for the QM part in the current system, the CASPT2(12,9) method is desirable, but the on-the-fly excited-state QM-MD or QM/MM-MD simulations employing CASPT2(12,9) are computationally prohibitive. The CASSCF method is often used for the on-the-fly excited-state MD simulations, but as seen below, the vertical excitation energy of the lowest $^1\pi\pi^*$ state at the CASSCF level is highly overestimated by ~2.0 eV, compared to that of CASPT2 or the experimental values. Since it is already suggested by many reports that in the gas phase the ^{1}nπ^* and $^1\pi\pi^*$ states are close in energy around the FC region, an accurate description of the both states is essential to provide a reliable picture of the deactivation process of thymine. Also, the CASSCF and CASPT2 calculations predict different electronic character of the $^1\pi\pi^*$ state at the respective minimum energy structure, leading to qualitatively different prediction of the decay mechanism.[24] Therefore, we employ the CASPT2 method for the MD simulations but with a reduced active space for reference SA-CASSCF wavefunctions: CASPT2(2,2) for the QM-MD simulations in the gas phase and CASPT2(4,4) for the QM/MM-MD simulations in aqueous solution. In both cases, only π orbitals are included in the active space, and the lowest three and lowest two states are averaged with equal weights in SA-CASSCF calculations for the CASPT2(2,2) and CASPT2(4,4) simulations, respectively. Along the MD trajectories, the CASPT2(12,9) calculations are performed at fixed time intervals to assess the accuracy of the CASPT2(2,2) or CASPT2(4,4) potential energies employed in the MD simulations. Employment of a different active space of (4,4) rather than (2,2) in the QM/MM-MD simulations is due to the fact that a significant deviation of the $^1\pi\pi^*$ potential energies from those of CASPT2(12,9) are observed occasionally when the CASPT2(2,2) method is used for the QM part, in particular when the molecule exhibits out-of-plane displacement of the carbonyl bond. On the other hand, when we employ (4,4) active space in the gas-phase simulation, the lone-pair orbital of the O8 atom enters into the active space and the electronic character of the S_1 state changes quickly from $^1\pi\pi^*$ to ^{1}nπ^* after photo-excitation to the $^1\pi\pi^*$ state. The ^{1}nπ^* state in the (4,4) active space, however, is not accurate since the CASPT2 potential energy of the ^{1}nπ^* state in the (12,9) active space differs considerably from that of the (4,4) active space. Obviously, our simulations focus on the deactivation process occurring only in the $^1\pi\pi^*$ state. Even so, the CASPT2(12,9) potential energies along the MD trajectories provide information regarding the role of the ^{1}nπ^* state in the deactivation process.

The Newtonian equation-of-motion for nuclei is integrated by the velocity Verlet algorithm with a time step of 0.5 fs. In order to prepare the initial conditions for the excited-state MD simulations, the constant temperature MD simulation is performed in the electronic ground state at the MP2 level of theory. The temperature is controlled at 300 K by the Nosé-Hoover thermostat. The initial coordinates and velocities used in the excited-state MD are taken from the above ground-state MD run by picking up coordinates and velocities at every 500 fs. The excited-state MD simulations are performed without the thermostats and they are initiated from the lowest $^1\pi\pi^*$ state. When the energy difference between the S_0 and $^1\pi\pi^*$ states becomes less than 0.2 eV, we assume that the molecule reaches the CI region. Of course, the evaluation of the transition probability is required for a more reliable description of the decay process, but unfortunately, a module for the analytical evaluation of the nonadiabatic coupling vectors at the CASPT2 level is not available in the current MOLPRO package. We note in passing that the efficient numerical calculation of the nonadiabatic coupling vectors at the MS-CASPT2 level in the framework of *ab initio* multiple spawning (AIMS) method has been proposed by Tao *et al.*[40] and also very recently the AIMS simulations with analytical evaluation of the nonadiabatic coupling vectors have been performed by Mori *et al.*[41] The on-the-fly excited-state MD simulations with nonadiabatic transitions at the MS-CASPT2 level for DNA bases will be feasible in the near future.

C. Absorption spectra in the gas phase and in aqueous solution

The absorption spectrum is obtained by plotting oscillator strength versus vertical excitation energy at geometries taken from the ground-state MD simulations at 100 fs time intervals. The vertical excitation energies are calculated at the CASPT2(12,9) level and the transition dipole moments at the SA-CASSCF(12,9) level are employed in obtaining the oscillator strength. A total of 50 configurations are picked up from each of the QM-MD (in the gas phase) and QM/MM-MD (in aqueous solution) simulations.

III. RESULTS AND DISCUSSION

A. Vertical excitation energies

The vertical excitation energies at the SA-CASSCF(12,9) and CASPT2(12,9) levels at the MP2-optimized structure $(S_0)_{min}$ (shown in Figure 1) are summarized in Table I, along with the recent literature values. As seen, the excitation energy to the lowest $^1\pi\pi^*$ state decreases appreciably upon inclusion of dynamic electron correlation by CASPT2, while the energy of the lowest ^{1}nπ^* state is almost unchanged. At the CASPT2(12,9) level, the lowest ^{1}nπ^* state is only slightly lower than the $^1\pi\pi^*$ state. As seen in previous studies,[17,18,26–35] the order of the lowest $^1\pi\pi^*$ and ^{1}nπ^* states changes depending on the computational levels. The literature values are well compiled in Ref. 23 and the recent values after Ref. 23 are included in Table I. It is seen that the CASPT2(12,9) excitation energy for the lowest $^1\pi\pi^*$ state is in very good agreement with the experimental value of 4.95 eV estimated from electron energy loss spectroscopy.[42] The lowest $^1\pi\pi^*$ excitation energy of CASPT2(2,2), which is used in the excited-state MD simulations, exhibits a good agreement with that of CASPT2(12,9). The active orbitals at

TABLE I. Vertical excitation energies (in eV) for low-lying singlet excited states. The number in parentheses represents the oscillator strength.

	$S_1(^1n\pi^*)$	$S_2(^1\pi\pi^*)$	$S_3(^1\pi\pi^*)$	$S_4(^1n\pi^*)$	Reference
SA-CASSCF(12,9)/DZP	4.84 (0.000)	6.75 (0.362)	7.16 (0.003)	7.75 (0.000)	This work
CASPT2(12,9)/DZP	4.82	4.83	5.95	6.99	This work
CASPT2(2,2)/DZP	...	4.90	...	...	This work
EOM-CCSD/6-311G**	5.25	5.69	6.94	6.70	23
CASPT2/6-31G*	5.11	5.38	6.60	6.57	23
RI-CC2/TZVPP	4.87	5.28	...	...	10
MS-CASPT2(10,8)/6-311G**	5.23	5.44	...	...	10
MR-SDCI/6-31G*	5.31	5.72	...	...	10
MS-CASPT2(12,9)/DZP	4.90	4.83	6.17	...	24
Experiments					
In gas[a]		4.95 ± 0.08	6.2 ± 0.08		42
In aqueous solution[b]		4.68			26

[a]Electron energy loss spectroscopy.
[b]Steady-state absorption spectroscopy.

$(S_0)_{min}$ in the SA-CASSCF(12,9) calculation are shown in the supplementary material (Figure S1).[43]

B. Potential energy profiles from $(S_0)_{min}$ to MECIs in the $^1\pi\pi^*$ state

The deactivation pathways through CI between the S_0 and $^1\pi\pi^*$ states are first explored by quantum chemical calculations. The MECI search is performed at the CASPT2 level and the low-lying three MECIs between the S_0 and $^1\pi\pi^*$ states are examined. The potential energy profiles from $(S_0)_{min}$ to each MECI are obtained using the linearly interpolated internal coordinate (LIIC) geometries.

The most common CI is of ethylene type that involves the twisting of the C5-C6 double bond with a strong puckering of the C6 atom. It is located as the lowest CI by several theoretical studies[8,10,21–23] and it is now generally accepted that the deactivation of thymine in the gas phase takes place almost exclusively through this CI. We performed the MECI search for this type of CI at the CASPT2(2,2) level. The use of this small active space is supported by the fact that the electronic configuration around this ethylene-like CI is well characterized by two π/π^* orbitals. The optimized structure is shown in Figure 2(a) and it is referred to as $(^1\pi\pi^*(C5\text{-}C6)/S_0)_{CI}$ hereafter. The natural orbitals relevant to the $^1\pi\pi^*$ excitation of this CI are given in Figure S2.[43] It exibits a large deformation of the six-membered ring and it is bent with respect to the N3-C6 axis, showing the butterfly conformation. The dihedral angle of *d*(N1-C6-C5-C9) representing the twisting of the C5-C6 double bond is −61.1° and the C5-C6 bond is elongated to 1.460 Å compared to that at the $(S_0)_{min}$ geometry (1.362 Å, see Figure 1). The CASPT2(12,9) potential energy profiles from $(S_0)_{min}$ to $(^1\pi\pi^*(C5\text{-}C6)/S_0)_{CI}$ along the LIIC path are shown in Figure 3(a). It exhibits a smooth downhill potential until reaching $(^1\pi\pi^*(C5\text{-}C6)/S_0)_{CI}$, and in fact the $^1\pi\pi^*$ geometry optimization starting from $(S_0)_{min}$ at the CASPT2(2,2) level leads to the $(^1\pi\pi^*(C5\text{-}C6)/S_0)_{CI}$ region and no minimum was found.

It should be noted here that the $^1\pi\pi^*$ minimum energy structure has been reported in the literature, where the

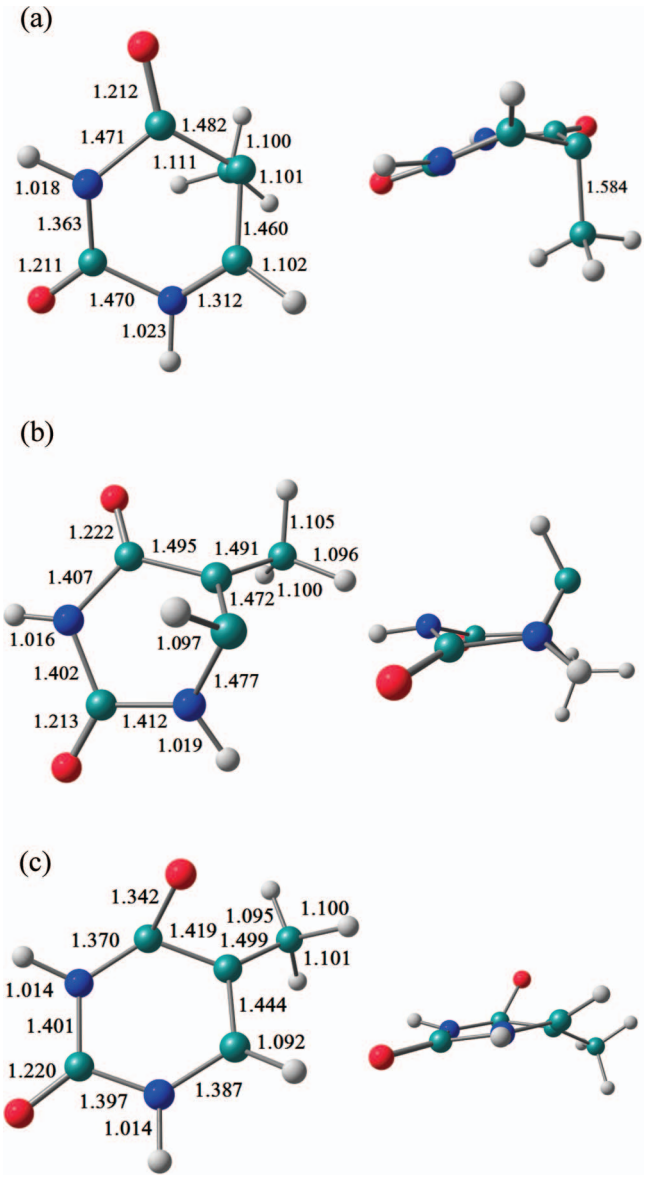

FIG. 2. MECI structures of (a) $(^1\pi\pi^*(C5\text{-}C6)/S_0)_{CI}$, (b) $(^1\pi\pi^*(C5\text{-}C6)/S_0)'_{CI}$, and (c) $(^1\pi\pi^*(C4\text{-}O8)/S_0)_{CI}$ for thymine. Bond lengths are given in units of Å.

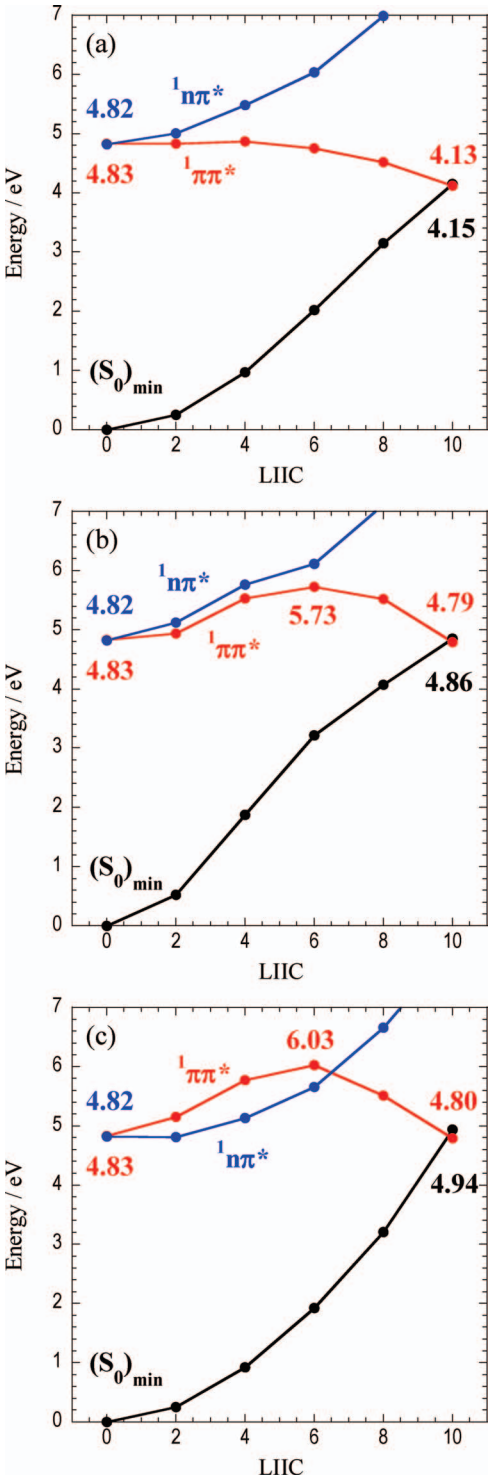

FIG. 3. Potential energy profiles from $(S_0)_{min}$ to (a) $(^1\pi\pi^*(C5\text{-}C6)/S_0)_{CI}$, (b) $(^1\pi\pi^*(C5\text{-}C6)/S_0)'_{CI}$, and (c) $(^1\pi\pi^*(C4\text{-}O8)/S_0)_{CI}$ using LIIC points at the CASPT2(12,9) level. The $^1\pi\pi^*$ energies at $(S_0)_{min}$, the highest point, and MECI structures are also shown.

CASSCF method has been mainly used for the geometry optimization.[7,8,10] At these CASSCF-optimized geometries, the electronic character involves a transition from the π(C4-O8) orbital to the π^*(C5-C6) orbital, which results in the elongation of both the C4-O8 and C5-C6 bonds relative to those at the $(S_0)_{min}$ structure. Since the potential energy curve from this $^1\pi\pi^*$ minimum to CI has a certain barrier height at the CASSCF level, dynamics simulations have predicted that the molecule spends some time around this minimum before reaching to CI and a picosecond decay has been attributed to this process.[7,10] However, the recent papers reported that the CASSCF-optimized minimum disappears in the CASPT2 calculations,[24,44] and the $^1\pi\pi^*$ minimum optimized by the CASPT2 method is characterized by the excitation of π(C5-C6) $\rightarrow$ π^*(C5-C6).[24] The CASPT2-optimized geometry involves the elongation of the C5-C6 bond while the C4-C8 bond length is almost unchanged. The energy barrier from this $^1\pi\pi^*$ minimum to CI was estimated to be less than 0.02 eV,[24] and therefore the picosecond decay could not be reconciled with an existence of this minimum. Although we could not locate the $^1\pi\pi^*$ minimum energy structure at the CASPT2(2,2) level, the CASPT2(2,2) potential energies show good agreement with those of CASPT2(12,9) (see Figure S3),[43] hence supporting the validity of using CASPT2(2,2) for the excited-state MD simulations.

According to the paper by Zechmann and Barbatti,[23] two other types of CI between the S_0 and $^1\pi\pi^*$ states have been reported. We locate these CIs at the CASPT2 level and investigate the potential energy profiles from $(S_0)_{min}$ to these CIs. One of these CIs involves also the twisting of the C5-C6 bond, where the MECI structure obtained at the CASPT2(2,2) level is shown in Figure 2(b). As seen, the pronounced deviation of the C6 atom from planarity is observed and the C5-C6 bond is elongated to 1.472 Å. This state exhibits a diradical character and it is described by a primary excitation from the *p* orbital on C6 to the *p* orbital of C5, which is opposite to that of $(^1\pi\pi^*(C5\text{-}C6)/S_0)_{CI}$ (the *p* orbital on C5 $\rightarrow$ the *p* orbital of C6). This structure is denoted as $(^1\pi\pi^*(C5\text{-}C6)/S_0)'_{CI}$ hereafter, where the prime is added to distinguish it from $(^1\pi\pi^*(C5\text{-}C6)/S_0)_{CI}$. The natural orbitals relevant to this excitation are given in Figure S4.[43] The CASPT2(12,9) energies at this point are 4.86 and 4.79 eV for the S_0 and $^1\pi\pi^*$ states, respectively, and these energies are very close to the $^1\pi\pi^*$ vertical excitation energy at $(S_0)_{min}$. The potential energy profiles from $(S_0)_{min}$ to $(^1\pi\pi^*(C5\text{-}C6)/S_0)'_{CI}$ are shown in Figure 3(b), and a significant barrier ($\sim$0.9 eV) is observed between the two structures. Therefore it is unlikely that this deactivation pathway is taken in reality, at least in the gas phase. It should be noted that the potential energy profiles along the LIIC coordinates are not the optimal deactivation pathways, and therefore the barrier height estimated from these profiles can be viewed as an upper bound for that of the minimum energy pathway. The relative energy at $(S_0)_{min}$ and MECI is a more important factor that determines the accessibility of CI after photo-excitation.

The other CI between the S_0 and $^1\pi\pi^*$ states is characterized by the out-of-plane displacement of the O8 atom. The MECI search at the CASPT2(2,2) level leads to CI between the S_0 and $^1n\pi^*$ states around this region, and therefore the CASPT2(4,4) method is instead employed for a MECI search, where only π/π^* orbitals are included in the active space. The resulting structure is shown in Figure 2(c), and it involves the deformation and also elongation of the C4-O8 bond, and the O8 atom is slightly directed toward the methyl group. The excitation at this structure is characterized by a transition from the π(C5-C6) bonding

orbital to the π^*(C4-O8) antibonding orbital, and therefore it is labeled as $(^1\pi\pi^*(\text{C4-O8})/S_0)_{CI}$ hereafter. The natural orbitals relevant to this excitation are given in Figure S5.[43] The CASPT2(12,9) energies at this point are calculated to be 4.94 and 4.80 eV for the S_0 and $^1\pi\pi^*$ states, respectively. The potential energy profiles from $(S_0)_{min}$ to $(^1\pi\pi^*(\text{C4-O8})/S_0)_{CI}$ are shown in Figure 3(c), and it exhibits a high barrier with a height of ~1.2 eV. Also, the $^1n\pi^*$ state lies below the $^1\pi\pi^*$ state along this pathway, and the molecule may switch to the $^1n\pi^*$ state before reaching this CI. Therefore, it is also unlikely that this pathway is taken in the gas phase, but as shown below in the excited-state dynamics simulations, the deactivation through this CI is observed in aqueous solution due to the stabilization of the $^1\pi\pi^*$ potential energies along this pathway.

In the supplementary material, the MECI geometries determined by MS-CASPT2 and the potential energy profiles from $(S_0)_{min}$ to the respective MECIs at the MS-CASPT2(12,9) level are shown in Figures S6 and S7,[43] along with the MS-CASPT2(12,9) effective Hamiltonian matrices and corresponding eigenvalues and eigenvectors at MECIs (Table SI). It is seen that the relative energies of the $^1\pi\pi^*$ state at $(S_0)_{min}$ and MECIs are similar in the (SS-)CASPT2 and MS-CASPT2 methods and that the diagonal elements of the transformation matrix are close to one for these states, which validates the use of the (SS-)CASPT2 method for the deactivation process in the $^1\pi\pi^*$ state.

C. Absorption spectra in the gas phase and in aqueous solution

Figure 4 shows the computed absorption spectra in the gas phase and in aqueous solution at the CASPT2(12,9) level using configurations taken from the ground-state MD simulations. In the gas phase (Figure 4(a)), the lowest $^1\pi\pi^*$ excitation energies are scattered over an energy range of approximately 0.5 eV, and the average over 50 configurations was calculated to be 4.80 eV, which is consistent with the vertical excitation energy of 4.83 eV at the ground-state equilibrium structure, $(S_0)_{min}$. The absorption spectrum for the lowest $^1n\pi^*$ band has a similar profile to that of $^1\pi\pi^*$, but the intensity is quite different since the oscillator strength for the $^1n\pi^*$ excitation is very weak compared to the $^1\pi\pi^*$ excitation (see Table I). For the $^1n\pi^*$ excitation, the average over 50 configurations was 4.74 eV. In aqueous solution (Figure 4(b)), the $^1\pi\pi^*$ absorption band is redshifted while the $^1n\pi^*$ band is blueshifted in comparison to the gas-phase results. For the $^1\pi\pi^*$ absorption band, the average over 50 samples was 4.48 eV and the shift from the gas phase value was −0.32 eV, which is in good agreement with the experimental observations, where the absorption maxima are 4.95 eV and 4.68 eV in the gas phase[42] and in aqueous solution,[26] respectively. The average of the $^1n\pi^*$ excitation energies was 5.46 eV and the blueshift of 0.72 eV from the gas-phase average was observed. The blueshift is primarily due to stabilization of a lone-pair orbital on O8 by hydrogen bonds with solvent water molecules. For the $^1n\pi^*$ band, a direct comparison to experimental results is not possible, but the calculated solvent shifts are in line with the

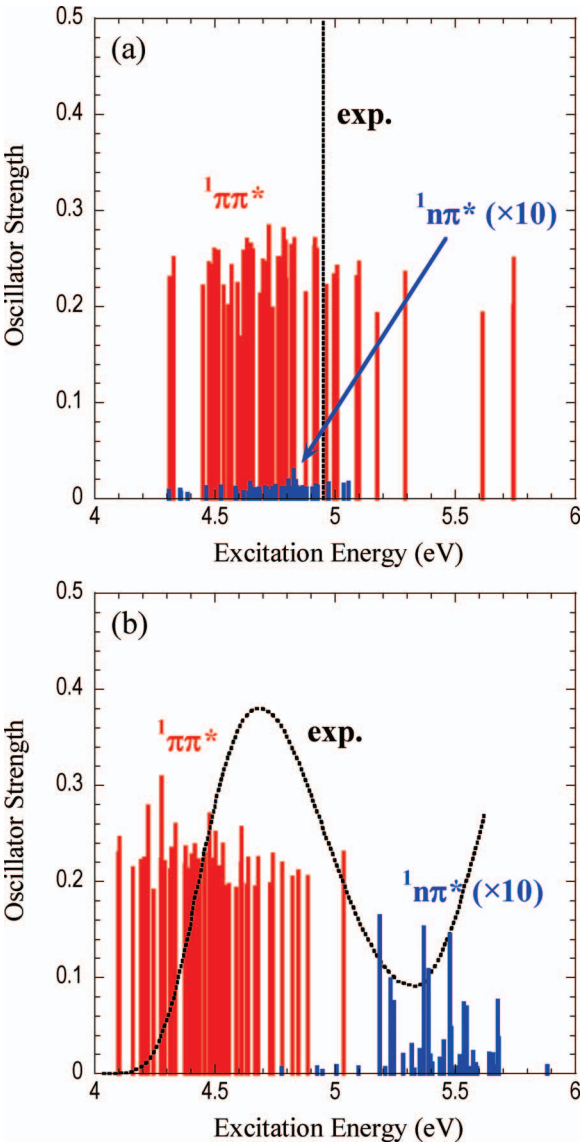

FIG. 4. Computed absorption spectra of thymine (a) in the gas phase and (b) in aqueous solution. Vertical lines are plots of oscillator strength versus excitation energy by CASPT2(12,9). The oscillator strength for the $^1n\pi^*$ transition is magnified 10 times as a guide to the eye. Experimental results are given in dotted lines; (a) vertical excitation energy from Ref. 42 is depicted as the vertical dotted line and (b) absorption spectrum in room-temperature aqueous solution taken from Ref. 26 is shown in arbitrary units.

time-dependent density functional theory (TD-DFT(PBE0)/6-311+G(2d,2p)) calculations using the polarizable continuum model (PCM) with an explicit inclusion of a small number of water molecules, where the shifts of −0.09 eV and 0.41 eV were reported for the $^1\pi\pi^*$ and $^1n\pi^*$ transitions, respectively.[26] In a similar calculation by TD-DFT(PBE0), Mercier *et al.*[44] estimated the shifts of −0.17 eV and +0.47 eV for the $^1\pi\pi^*$ and $^1n\pi^*$ transitions, respectively. We could not find literatures for absorption spectrum of thymine in aqueous solution in the framework of QM/MM approach, but our calculated solvatochromic shifts are in good agreement with the recent reports on uracil in aqueous solution, where the shifts of −0.29 eV and 0.45 eV for the $^1\pi\pi^*$ and $^1n\pi^*$ transitions have been reported, respectively, using a self-consistent polarizable model in the QM/MM-MD

TABLE II. Shifts of the $^1\pi\pi^*$ and $^1n\pi^*$ vertical excitation energies (in eV) of thymine and uracil due to solvation by water.

	ΔE ($^1\pi\pi^*$)	ΔE ($^1n\pi^*$)	Reference
Thymine			
CASPT2(12,9) in QM/MM	−0.32	+0.72	This work
TD-DFT(PBE0) in PCM	−0.09	+0.41	26
TD-DFT(PBE0) in PCM	−0.17	+0.47	44
Uracil			
CC2 in QM/MM	−0.29	+0.45	45
MCQDPT in QM/MM	−0.26	+0.43	46

simulations.[45] Also shifts of −0.26 eV and 0.43 eV have been predicted by the multiconfigurational quasidegenerate perturbation theory (MCQDPT) method combined with the effective fragment potential (EFP) solvent method.[46] These literature values are compiled in Table II.

As described above, the overall agreements with other theoretical studies[26,44–46] validate the accuracy of not only the *ab initio* method by CASPT2 but also the QM/MM treatment for surrounding solvent water molecules. In our simulations, the $^1\pi\pi^*$ state is lower in energy than $^1n\pi^*$ by ∼1.0 eV in aqueous solution.

D. QM-MD simulations in the gas phase

We start with the results of the excited-state QM-MD simulations in the gas phase. A total of ten trajectories were launched from the lowest $^1\pi\pi^*$ state, and it was found that in all trajectories the molecule reached the CI region of the $(^1\pi\pi^*(C5\text{-}C6)/S_0)_{CI}$ type which involves the twisting of the C5-C6 bond.

Figure 5(a) shows the time evolution of the CASPT2(2,2) potential energies along a representative trajectory, and the CASPT2(12,9) potential energies are also plotted at selected points along the trajectory. Note that the excited-state MD simulations were performed using CASPT2(2,2) potential energies and analytical gradients for reducing the computational cost, and the CASPT2(12,9) calculations were carried out to assess the accuracy of the CASPT2(2,2) potential energies. In this CASPT2(2,2) trajectory, potential energies of the S_0 and $^1\pi\pi^*$ states become almost identical at ∼0.28 ps, suggesting that the molecule reaches the CI region. Time variation of characteristic geometrical parameters is given in Figure 5(b), and as seen the dihedral angle of *d*(N1-C6-C5-C9) representing the twisting of the C5-C6 double bond gradually increases as the molecule moves toward this CI. The C5-C6 bond is elongated right after the excitation at $t = 0$, which is consistent with the excitation character involving a transition of π(C5-C6) → π^*(C5-C6), and then it oscillates around 1.47 Å

The CASPT2(12,9) energies of the $^1\pi\pi^*$ state along the trajectory show very good agreement with those of CASPT2(2,2). When the molecule is photo-excited at $t = 0$, the $^1\pi\pi^*$ and $^1n\pi^*$ states are close in energy, which is reflected in the absorption spectrum shown above. However, as seen in the CASPT2(12,9) energies along the trajectory, the $^1n\pi^*$ state is destabilized quickly in the course of dynamics in the $^1\pi\pi^*$ state and it does not come into play later in the deactivation process. Although a transition to $^1n\pi^*$ is not taken into account in the present simulations, the results suggest that the fate of a trajectory whether the molecule deactivates directly through the $^1\pi\pi^*$ state or switches to $^1n\pi^*$ would be determined in the very early stage of the dynamics.

In all ten trajectories, it was observed that the molecule reached this type of CI in the range of 0.18–0.70 ps as in the same manner in the representative trajectory shown above. The average of that time over 10 trajectories was given as 0.40 ps. Note that it does not mean that the transition to the ground state takes place at this time since the nonadiabatic transition is not taken into account in the present simulation. At least the existence of CI is predicted around this region and the molecule would deactivate to the ground state in the similar timescale.

Here we should comment on related works. In CASSCF-based MD simulations, the molecule spends relatively long time in the $^1\pi\pi^*$ state since there is a minimum in the CASSCF potential energy surface.[7,8,10,47] For example, Szymczak *et al.* estimated a time constant of 2.6 ps for the deactivation from the $^1\pi\pi^*$ state.[10] However, this type of minimum disappears in the CASPT2 potential energy surfaces, and in fact the CASPT2(2,2) potential energy profiles exhibit no minimum in the $^1\pi\pi^*$ state. Although a very shallow minimum was predicted by the more elaborated MS-CASPT2 calculations (note that this minimum possesses a different electronic excitation character from that obtained by CASSCF),[24] a fast quenching within several hundreds femtoseconds is a plausible mechanism.

E. QM/MM-MD simulations in aqueous solution

In the excited-state QM/MM-MD simulations in aqueous solution, a total of ten trajectories were also launched from the $^1\pi\pi^*$ state and all trajectories reached the CI region within 1 ps. In seven trajectories out of ten the molecule encountered the $(^1\pi\pi^*(C5\text{-}C6)/S_0)_{CI}$ region, and very interestingly, we found that in the other three trajectories the molecule reached the $(^1\pi\pi^*(C4\text{-}O8)/S_0)_{CI}$ region which accompanies the out-of-plane displacement of the carbonyl group.

First, the results of a representative trajectory reaching the $(^1\pi\pi^*(C5\text{-}C6)/S_0)_{CI}$ region are presented. Figure 5(c) shows the time evolution of the CASPT2(4,4) potential energy that is defined as a sum of the electronic energy of the thymine molecule (QM) and the electrostatic interaction energy between the QM and MM molecules. Compared to the gas-phase results in Figure 5(a), the potential energy exhibits a large fluctuation due to the electrostatic interaction with solvent water molecules. In this trajectory, the molecule reached the CI region at ∼0.18 ps. The geometrical changes are similar to those in the gas phase calculations (see Figure 5(d)), but we notice that the C4-O8 bond length is slightly elongated due to the hydrogen-bond interactions with solvent molecules. The CASPT2(12,9) potential energies agree fairly well with the CASPT2(4,4) results for the $^1\pi\pi^*$ state. As seen in the CASPT2(12,9) energies, the $^1n\pi^*$ state lies above the $^1\pi\pi^*$

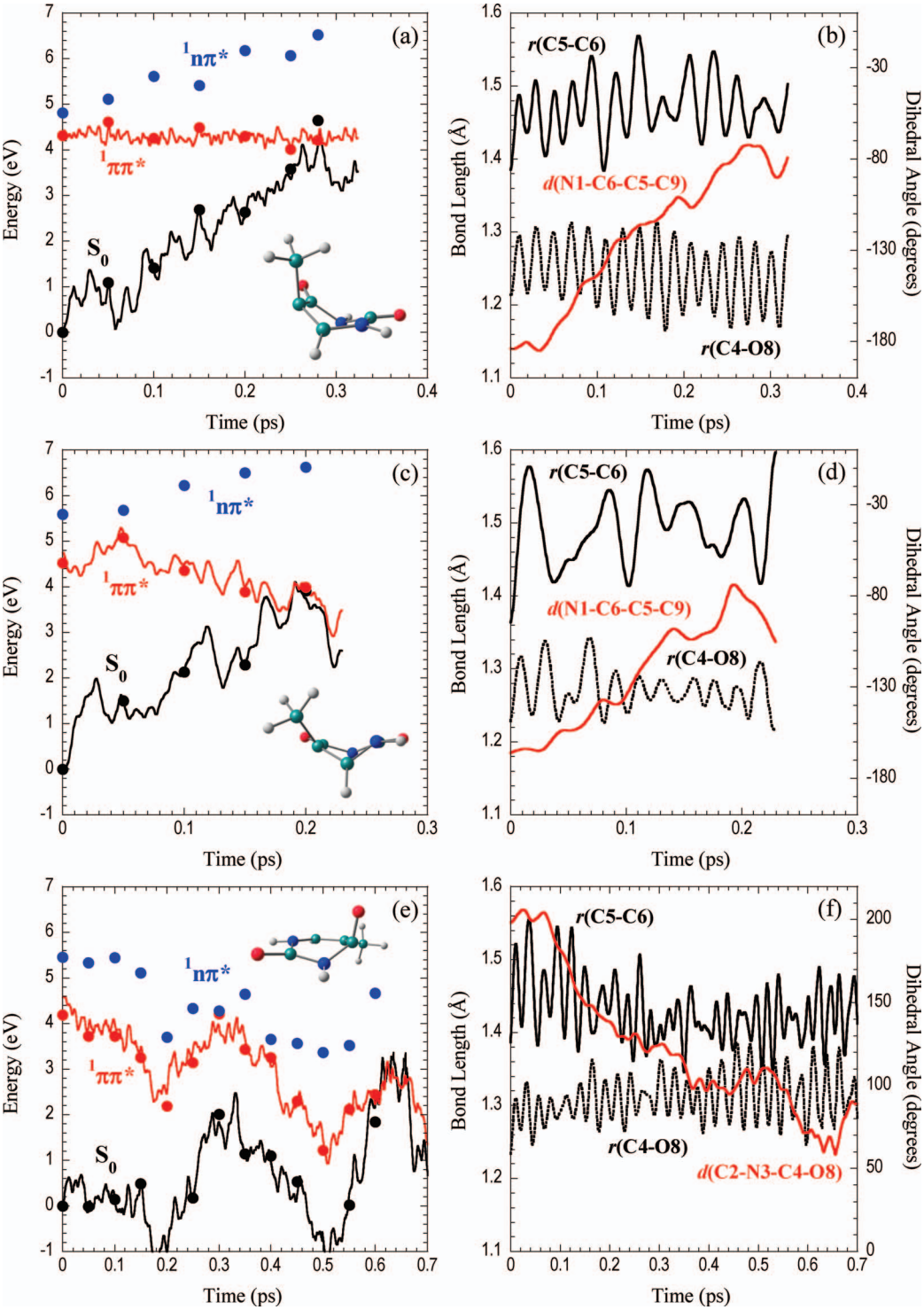

FIG. 5. (a) CASPT2(2,2) potential energies (solid lines) and (b) geometrical parameters along a representative trajectory in the QM-MD simulations. (c, e) CASPT2(4,4) potential energies (solid lines) and (d, f) geometrical parameters along a representative trajectory that reaches $(^1\pi\pi^*(\text{C5-C6})/S_0)_{CI}$ and $(^1\pi\pi^*(\text{C4-O8})/S_0)_{CI}$ regions in the QM/MM-MD simulations, respectively. The CASPT2(12,9) energies are included at selected points along the trajectory (filled circles). The zero is set to the ground-state potential energy at $t = 0$, where the excited-state MD simulation is started. Molecular structures around the CI region are also shown.

state by more than 1 eV for most of the simulation time. Even at $t = 0$ when the molecule is photo-excited, the $^1n\pi^*$ state lies more than 1 eV higher than the $^1\pi\pi^*$ state, which is reflected in the absorption spectra in Figure 4(b). This result indicates that only the $^1\pi\pi^*$ state would be relevant in the deactivation process of thymine in aqueous solution. A similar trend was observed in the other six trajectories, and the molecule reached the CI region in the range of 0.16–0.65 ps and the average was given as 0.31 ps, which is similar to the gas-phase value.

Figures 5(e) and 5(f) show the time dependent profiles of the CASPT2(4,4) potential energy and geometrical parameters along a representative trajectory that reached the $(^1\pi\pi^*(\text{C4-O8})/S_0)_{CI}$ region at ~0.60 ps. In contrast to the trajectories reaching $(^1\pi\pi^*(\text{C5-C6})/S_0)_{CI}$, the C5-C6 bond length gradually decreases after an increase at $t = 0$, while the C4-O8 bond length increases to around 1.32 Å as time proceeds. This behavior coincides with the geometrical changes observed in the deactivation pathway leading to $(^1\pi\pi^*(\text{C4-O8})/S_0)_{CI}$ since it involves the excitation of $\pi(\text{C5-C6}) \rightarrow \pi^*(\text{C4-O8})$. The dihedral angle of d(C2-N3-C4-O8) that characterizes the C4-O8 bond distortion from the ring plane also signifies this process. The other two trajectories reached the CI region at 0.23 and 0.59 ps.

As seen in Figure 3(c), the $^1\pi\pi^*$ potential energy at $(^1\pi\pi^*(\text{C4-O8})/S_0)_{CI}$ (~4.9 eV) and barrier for pathway leading to this CI (~1.2 eV) are quite high in energy in the gas phase calculation. Our simulation data suggest that the electrostatic interaction with the solvent water molecules stabilizes the potential energies along this pathway significantly. In order to clarify the solvent effects, the potential energies of isolated thymine are calculated at selected geometries along the QM/MM-MD trajectories by ignoring the MM water molecules, and compared with the QM/MM potential energies of the solvated system. Figure 6 shows the potential energy difference between the $^1\pi\pi^*$ and S_0 states ($\Delta E = E(^1\pi\pi^*) - E(S_0)$) at the CASPT(12,9) level along the representative trajectories leading to the (i) $(^1\pi\pi^*(\text{C5-C6})/S_0)_{CI}$ and (ii) $(^1\pi\pi^*(\text{C4-O8})/S_0)_{CI}$ regions (the same trajectories given in Figures 5(c) and 5(e), respectively).

In trajectory (i), it is seen that the profiles of potential energy difference (dotted lines in Figure 6) are relatively similar in two cases: with and without MM water molecules. Even without the water molecules, the potential energy difference is only ~0.8 eV around the $(^1\pi\pi^*(\text{C5-C6})/S_0)_{CI}$ region. For trajectory (ii), in contrast, the potential energy profiles are quite different in the two cases (solid lines in black and red, respectively). In particular, without the MM solvent molecules, the potential energy difference is still large around the CI region (~2.5 eV). This figure clearly demonstrates that the solvent water molecules stabilize the potential energies along the pathway to $(^1\pi\pi^*(\text{C4-O8})/S_0)_{CI}$ significantly, and it is also suggested that the configuration of the CI seam is altered by the electrostatic interaction.

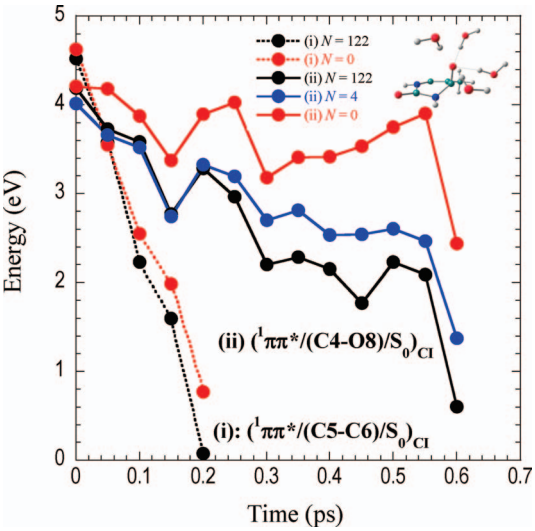

FIG. 6. Potential energy difference between the $^1\pi\pi^*$ and S_0 states at the CASPT2(12,9) level along the representative trajectories given in Figures 5(c) and 5(e) labeled as (i) and (ii), respectively. The black line represents the result with all solvent water molecules (122 molecules) and the red line shows the result without solvent molecules. The blue line indicates the result with only four water molecules that are hydrogen-bonded to the O8 atom.

It is also interesting to elucidate the effects of solute-solvent hydrogen bonds in trajectory (ii) and they are investigated in the following way: the potential energies are calculated for thymine with selected MM water molecules that are hydrogen-bonded to the O8 atom along the same QM/MM-MD trajectory. Four MM water molecules are employed for this investigation, and they are chosen since the distance between O8 and hydrogen atom of these MM water molecules becomes less than 2.0 Å at some points during the simulation. The calculated energy profiles are shown as the blue solid line in Figure 6. As seen in the figure, these four water molecules stabilize the potential energy profiles appreciably. This result can be explained by the fact that the excitation involves an electronic transition to the π^*(C4-O8) orbital and that this orbital is stabilized by the hydrogen bonds with the solvent water molecules. In this way it is clearly seen that the hydrogen bonds play a key role in the deactivation through $(^1\pi\pi^*(\text{C4-O8})/S_0)_{CI}$.

We note in passing that similar types of CIs were reported previously for other DNA/RNA bases (i.e., cytosine,[11] uracil,[48] and guanine[49–53]), where significant displacement of oxygen atom in the carbonyl group from molecular plane is observed. In particular, the deactivation through this type of CI was observed for guanine in aqueous solution by the QM/MM simulations at the semiempirical OM2/MRCI level, while in the gas phase it did not play any significant role.[53] The appearance of this additional CI in guanine might be attributed to the same mechanism as discussed above for thymine.

In the femtosecond UV fluorescence upconversion experiments in various solvents,[26–28] the authors found that there is no direct correlation between the excited-state lifetimes and macroscopic parameters such as polarity or viscosity, but they suggested that the hydrogen bonds between thymine and solvent molecules play an important role in determining the fluorescence decay rate. They discussed this solvent dependence based on the relative stability of the $^1\pi\pi^*$ and $^1n\pi^*$ states since it affects the efficiency of population transfer to the dark $^1n\pi^*$ state. In the present work, we propose that in aqueous solution only the $^1\pi\pi^*$ state is involved in the deactivation process and that there would be a nonnegligible contribution of this newly found pathway to the observed decay profiles. Unfortunately, our limited statistics do not allow the quantitative estimates of the ratio of these two deactivation pathways in the $^1\pi\pi^*$ state and also the average decay time for each pathway. It takes about one month to run the simulation time of 0.5 ps for each QM/MM-MD simulation, and therefore at present it is a demanding task to compare with the experimental results.

IV. CONCLUSIONS AND FUTURE DIRECTIONS

We performed the on-the-fly excited-state MD simulations of thymine in the gas phase and in aqueous solution, mainly focusing on the role of solvent water molecules on the deactivation process in the $^1\pi\pi^*$ state. Most of the previous on-the-fly excited-state dynamics simulations are based on the CASSCF, TD-DFT, or semiempirical methods for electronic structure calculations, but in this work the CASPT2 method was employed in order to provide a more reliable description of the excited-state potential energies.

In the gas phase calculations, it was found that all trajectories encounter the CI region involving the twisting of the C5-C6 double bond in the range of 0.18–0.70 ps. It was also found that the $^1n\pi^*$ state was destabilized quickly in the course of dynamics in the $^1\pi\pi^*$ state. In aqueous solution, the absorption spectra indicate that the $^1n\pi^*$ band lies higher than that of the $^1\pi\pi^*$ state with an average difference of ∼1.0 eV. The excited-state QM/MM-MD simulations showed that in 7 trajectories out of 10 reached the same type of CI region as in the gas phase. The important finding of the present work is that in aqueous solution three trajectories out of 10 encountered the CI that was not observed in the gas phase simulations. Our analysis indicates that the hydrogen bonds with solvent water molecules stabilize the $^1\pi\pi^*$ state involving the π(C5-C6) → π^*(C4-O8) excitation, which leads to the opening of this additional efficient deactivation pathway. Thus, this CI may play a significant role in the deactivation process of thymine in aqueous solution. Another important finding of the present work is that in aqueous solution only the $^1\pi\pi^*$ state would be involved in the deactivation process.

On-the-fly excited-state MD simulations are powerful tool to investigate the intricate deactivation mechanisms of DNA bases, in particular, in complex environments. The solvent effects of other polar solvents such as acetonitrile or alcohols on the relaxation process will be investigated in the near future, including the quantitative estimates of lifetime constants by the improved statistics, in order to provide a more comprehensive picture of the deactivation mechanics of thymine in the condensed phase. The substitution effects on the C5 atom also remain the subjects of future investigation, where the different solvent dependence is observed depending on the C5-substitution.[26–28] We are also currently investigating the effects of complex environments such as base-pair and base-stacking interactions, which are seen in double-stranded nucleic acids in DNA environments. These topics will be addressed in future studies in the framework of excited-state QM/MM-MD approach.

ACKNOWLEDGMENTS

The authors acknowledge the financial support by KAKENHI (Grant-in-Aid for Scientific Research). S.Y. thanks the Japan Society for the Promotion of Science (JSPS) for the Research Fellowships for Young Scientists. The authors thank Mr. Masayuki Okai for performing some additional calculations. Part of the calculations was performed on supercomputers at Research Center for Computational Science, Okazaki, Japan.

[1] C. E. Crespo-Hernández, B. Cohen, P. M. Hare, and B. Kohler, Chem. Rev. **104**, 1977 (2004).
[2] B. Kohler, Photochem. Photobiol. **83**, 592 (2007).
[3] H. Saigusa, J. Photochem. Photobiol. C **7**, 197 (2006).
[4] B. Kohler, J. Phys. Chem. Lett. **1**, 2047 (2010).
[5] W. Domcke, D. R. Yarkony, and H. Köppel, *Conical Intersections: Theory, Computation and Experiment* (World Scientific, Singapore, 2011).
[6] M. K. Shukla and J. Leszczynski, *Radiation Induced Molecular Phenomena in Nucleic Acids* (Springer-Verlag, Berlin, 2008).
[7] H. R. Hudock, B. G. Levine, A. L. Thompson, H. Satzger, D. Townsend, N. Gador, S. Ullrich, A. Stolow, and T. J. Martínez, J. Phys. Chem. A **111**, 8500 (2007).
[8] D. Asturiol, B. Lasorne, M. A. Robb, and L. Blancafort, J. Phys. Chem. A **113**, 10211 (2009).
[9] Z. Lan, E. Fabiano, and W. Thiel, J. Phys. Chem. B **113**, 3548 (2009).
[10] J. J. Szymczak, M. Barbatti, J. T. Soo Hoo, J. A. Adkins, T. L. Windus, D. Nachtigallová, and H. Lischka, J. Phys. Chem. A **113**, 12686 (2009).
[11] M. Barbatti, A. J. A. Aquino, J. J. Szymczak, D. Nachtigallova, and H. Lischka, Phys. Chem. Chem. Phys. **13**, 6145 (2011).
[12] H. Kang, K. T. Lee, B. Jung, Y. J. Ko, and S. K. Kim, J. Am. Chem. Soc. **124**, 12958 (2002).
[13] Y. He, C. Wu, and W. Kong, J. Phys. Chem. A **107**, 5145 (2003).
[14] Y. He, C. Wu, and W. Kong, J. Phys. Chem. A **108**, 943 (2004).
[15] S. Ullrich, T. Schultz, M. Z. Zgierski, and A. Stolow, Phys. Chem. Chem. Phys. **6**, 2796 (2004).
[16] C. Canuel, M. Mons, F. Piuzzi, B. Tardivel, I. Dimicoli, and M. Elhanine, J. Chem. Phys. **122**, 074316 (2005).
[17] E. Samoylova, H. Lippert, S. Ullrich, I. V. Hertel, W. Radloff, and T. Schultz, J. Am. Chem. Soc. **127**, 1782 (2005).
[18] E. Samoylova, T. Schultz, I. V. Hertel, and W. Radloff, Chem. Phys. **347**, 376 (2008).
[19] J. González-Vázquez, L. González, E. Samoylova, and T. Schultz, Phys. Chem. Chem. Phys. **11**, 3927 (2009).
[20] P. M. Hare, C. E. Crespo-Hernández, and B. Kohler, Proc. Natl. Acad. Sci. U.S.A. **104**, 435 (2007).
[21] S. Perun, A. L. Sobolewski, and W. Domcke, J. Phys. Chem. A **110**, 13238 (2006).
[22] M. Merchán, R. González-Luque, T. Climent, L. Serrano-Andrés, E. Rodríguez, M. Reguero, and D. Peláez, J. Phys. Chem. B **110**, 26471 (2006).
[23] G. Zechmann and M. Barbatti, J. Phys. Chem. A **112**, 8273 (2008).
[24] S. Yamazaki and T. Taketsugu, J. Phys. Chem. A **116**, 491 (2012).
[25] J. J. Serrano-Pérez, R. González-Luque, M. Merchán, and L. Serrano-Andrés, J. Phys. Chem. B **111**, 11880 (2007).
[26] T. Gustavsson, Á. Bányász, E. Lazzarotto, D. Markovitsi, G. Scalmani, M. J. Frisch, V. Barone, and R. Improta, J. Am. Chem. Soc. **128**, 607 (2006).
[27] T. Gustavsson, N. Sarkar, Á. Bányász, D. Markovitsi, and R. Improta, Photochem. Photobiol. **83**, 595 (2007).
[28] T. Gustavsson, Á. Bányász, N. Sarkar, D. Markovitsi, and R. Improta, Chem. Phys. **350**, 186 (2008).
[29] B. G. Levine, J. D. Coe, and T. J. Martínez, J. Phys. Chem. B **112**, 405 (2008).
[30] See http://setani.sci.hokudai.ac.jp/sapporo/ for information about the Sapporo basis set.
[31] K. Andersson, P. A. Malmqvist, B. O. Roos, A. J. Sadlej, and K. Wolinski, J. Phys. Chem. **94**, 5483 (1990).
[32] P. Celani and H.-J. Werner, J. Chem. Phys. **112**, 5546 (2000).
[33] J. Finley, P.-Å. Malmqvist, B. O. Roos, and L. Serrano-Andrés, Chem. Phys. Lett. **288**, 299 (1998).
[34] A. Nakayama, Y. Harabuchi, S. Yamazaki, and T. Taketsugu, Phys. Chem. Chem. Phys. **15**, 12322 (2013).
[35] L. Serrano-Andrés, M. Merchán, and R. Lindh, J. Chem. Phys. **122**, 104107 (2005).
[36] B. O. Roos and K. Andersson, Chem. Phys. Lett. **245**, 215 (1995).
[37] H.-J. Werner, P. J. Knowles, R. Lindh, F. R. Manby, M. Schütz *et al.*, MOLPRO, version 2008.1, a package of *ab initio* programs, 2008, see http://www.molpro.net.
[38] Y. Wu, H. L. Tepper, and G. A. Voth, J. Chem. Phys. **124**, 024503 (2006).
[39] P. Celani and H.-J. Werner, J. Chem. Phys. **119**, 5044 (2003).
[40] H. Tao, B. G. Levine, and T. J. Martínez, J. Phys. Chem. A **113**, 13656 (2009).
[41] T. Mori, W. J. Glover, M. S. Schuurman, and T. J. Martinez, J. Phys. Chem. A **116**, 2808 (2012).
[42] R. Abouaf, J. Pommier, and H. Dunet, Chem. Phys. Lett. **381**, 486 (2003).

[43]See supplementary material at http://dx.doi.org/10.1063/1.4833563 for active orbitals, natural orbitals at MECIs, and potential energy profiles.
[44]Y. Mercier, F. Santoro, M. Reguero, and R. Improta, J. Phys. Chem. B **112**, 10769 (2008).
[45]J. M. Olsen, K. Aidas, K. V. Mikkelsen, and J. Kongsted, J. Chem. Theory Comput. **6**, 249 (2010).
[46]A. DeFusco, J. Ivanic, M. W. Schmidt, and M. S. Gordon, J. Phys. Chem. A **115**, 4574 (2011).
[47]D. Asturiol, B. Lasorne, G. A. Worth, M. A. Robb, and L. Blancafort, Phys. Chem. Chem. Phys. **12**, 4949 (2010).
[48]S. Matsika, J. Phys. Chem. A **108**, 7584 (2004).
[49]C. M. Marian, J. Phys. Chem. A **111**, 1545 (2007).
[50]L. Serrano-Andrés, M. Merchán, and A. C. Borin, J. Am. Chem. Soc. **130**, 2473 (2008).
[51]Z. Lan, E. Fabiano, and W. Thiel, ChemPhysChem **10**, 1225 (2009).
[52]M. Barbatti, J. J. Szymczak, A. J. A. Aquino, D. Nachtigallova, and H. Lischka, J. Chem. Phys. **134**, 014304 (2011).
[53]B. Heggen, Z. Lan, and W. Thiel, Phys. Chem. Chem. Phys. **14**, 8137 (2012).